HERO: A SPACE-BASED LOW FREQUENCY INTERFEROMETRIC OBSERVATORY FOR HELIOPHYSICS ENABLED BY NOVEL VECTOR SENSOR TECHNOLOGY

M. Knapp*, D. E. Gary†, M. H. Hecht‡, C. Lonsdale‡, F. D. Lind‡,
F. C. Robey§, L. Fuhrman§, B. Chen¶, A. J. Fenn§,
and the HeRO team‖

Abstract

HeRO (Heliophysics Radio Observer) is a hybrid ground and space mission concept for radio interferometry of solar radio bursts. The space segment (HeRO-S) covers low frequencies, 100 kHz–20 MHz, and is composed of 6 free–flying CubeSats equipped with vector sensors. The ground segment (HeRO-G), covers higher frequencies, 15 MHz–300 MHz. HeRO will explore conditions and disturbances in a key region of the heliosphere, from two to tens of solar radii, using interferometric observations of solar radio bursts over three decades in frequency. Spot mapping across the full frequency range will provide precise positions and basic structural information about type II and III radio bursts. The morphology of CME shock fronts will be traced via type II burst emissions, and heliospheric magnetic field geometries will be probed by measuring precise trajectories of type III bursts. Refraction in the heliospheric plasma on large and intermediate scales will be investigated throughout large volumes via the frequency dependence of accurate interferometric positional data on bursts. The HeRO data will be information rich with high resolution in time, frequency and spatial position, and high SNR, creating fertile ground for discovery of new phenomena.

* *Department of Earth, Atmospheric, and Planetary Science, MIT, Cambridge, MA, USA*
† *Mission PI, Center for Solar–Terrestrial Research, New Jersey Institute of Technology, NJ, USA*
‡ *MIT Haystack Observatory, Westford, MA, USA*
§ *MIT Lincoln Laboratory, Lexington, MA, USA*
¶ *Center for Solar–Terrestrial Research, New Jersey Institute of Technology, NJ, USA*
‖ *see Acknowledgments*

This material is based upon work supported by the Assistant Secretary of Defense for Research and Engineering under Air Force Contract No. FA8721-05-C-0002 and/or FA8702-15-D-0001. Any opinions, findings, conclusions or recommendations expressed in this material are those of the author(s) and do not necessarily reflect the views of the Assistant Secretary of Defense for Research and Engineering.

1 Introduction

The Sun, our star, is a powerful source of non-thermal radio emission. Solar radio bursts provide insight into the Sun's magnetic field, coronal processes, and the solar wind. A wide range of spacecraft (e.g. SOHO [Domingo et al., 1995], SDO [Pesnell et al., 2012], STEREO [Kaiser et al., 2008]) and ground-based instruments (e.g. Owens Valley Solar Array [Gary and Hurford, 1994], LOFAR [Mann et al., 2011]) monitor the Sun at radio wavelengths and across the electromagnetic spectrum in order to understand heliophysical processes. These observatories also contribute to forecasting potentially dangerous space weather that can wreak havoc on navigation, communications, and power grids. This paper describes HeRO (**He**liophysics **R**adio **O**bserver), a hybrid ground and space instrument to map and track type II and III solar radio bursts as they propagate from the solar corona out into the interplanetary medium. HeRO will be capable of tracking type II and III radio bursts with unprecedented spatial resolution through the use of multi–baseline radio interferometry from 300 MHz to 100 kHz.

2 HeRO science

The solar corona, the solar wind, and the interplanetary medium are natural environments that enable the study of fundamental plasma physics. HeRO will observe radio emissions generated in the heliospheric plasma environment to address three science objectives:

1. Determine the location, shape, and properties of coronal and interplanetary shocks
2. Determine the site and conditions for efficient particle acceleration
3. Trace open magnetic fields along which energetic particles propagate

These objectives can be addressed by remote observation of type II and III radio bursts across frequency (and corresponding solar distance) with high temporal and spatial resolution. Figure 1 shows that HeRO (composed of ground-based HeRO-G and space-based HeRO-S) will track solar radio bursts from the corona (1.03 R_{Sun}) to 0.5 AU (90 R_{Sun}).

2.1 Type II and III solar radio bursts

When the effects of a coronal mass ejection (CME) accelerate already–energized electrons present in the ambient plasma, the resulting type II emission reflects the morphology and motion of both the shock front and the CME, as well as the geometry of the local magnetic field. Detectable type II bursts occur a few times per month, radiating both at the fundamental and the second harmonic of the local plasma frequency. As the disturbance propagates outward into lower density plasma, the emission drifts from higher to lower frequency with typical timescales of minutes to hours. Note that some diffuse type II–like bursts may be due to gyrosynchrotron emission, rather than plasma emission, although this remains speculative [Bastian, 2007; Pohjolainen et al., 2013].

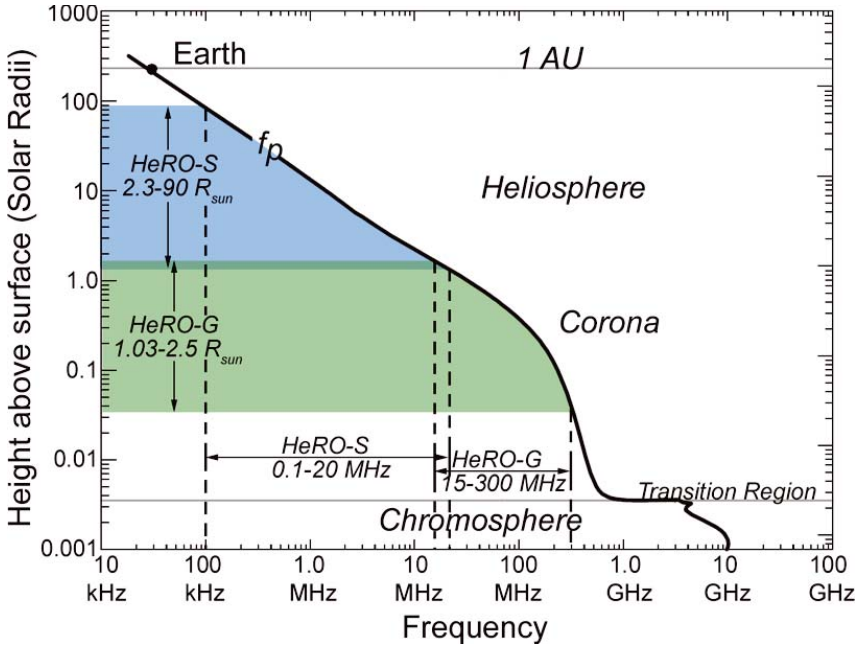

Figure 1: Plasma frequency as a function of solar distance (see Gary et al., 2004; references therein). The green shaded portion of the plot shows HeRO-G coverage. The blue shaded area shows HeRO-S coverage. HeRO (HeRO-S + HeRO-G) covers 100 kHz–300 MHz in frequency and 1.03–90 R_{Sun}.

Type III bursts are brief, lasting seconds to minutes, but are much more common than type IIs. Magnetic reconnection events accelerate energetic electrons across a broad range of heliocentric distances, resulting in fast moving 'beams' of electrons propagating along magnetic field lines at appreciable fractions of the speed of light. These beams radiate at the fundamental and second harmonic with a broad distribution of starting frequencies, drifting rapidly to lower frequencies.

The burst phenomena to be studied by HeRO are initiated close to the solar surface and propagate far out into interplanetary space. HeRO will enable tracking both type II–producing shock waves and type III–producing electron beams along this full range of distances. For type II bursts, HeRO will follow the evolution of the radio–emitting regions (objective 1) due to electron acceleration. These regions are presumably the sites of ion acceleration as well, so tracking them as they evolve will provide a better understanding of how the shock parameters (speed, Mach number, magnetic field geometry) affect the conditions of efficient acceleration (objective 2). HeRO, with its wide frequency coverage, will track the entire life–cycle of the shock, in particular the 'hot spots' of particle acceleration at its front or flank, from the time the radio emission first develops in the low corona, transits the mainly–closed–field regions below the 'source surface' [Culhane et al., 2014], enters the solar–wind–dominated region, and then sweeps through ever larger portions of the heliosphere.

For type III bursts, we are mainly interested in defining the radio–emitting electron beam trajectories throughout their lifetimes. By remotely measuring the precise emission location as the type III burst propagates outward, the magnetic field line along which the

electron beam is propagating can be mapped. A full understanding of these events, and the answers to the science questions posed, demands observations spanning the full range of frequency from event initiation to the limits imposed by the plasma frequency at the HeRO-S orbit. In practice, this means from a few hundred MHz to 100 kHz. Consequently, HeRO is designed to operate across this full range simultaneously, with no gaps, from 100 kHz to 300 MHz. Because the radio emission is due to plasma emission, there is a one–to–one correspondence between emitting frequency and distance from the Sun (Figure 1).

2.2 Spot mapping

Using radio interferometry techniques, HeRO will measure the location of type II and type III burst emissions with ∼20 to 2000 times better accuracy than current space-based instruments, depending on frequency, and with both improved precision and wider frequency coverage than current ground-based instruments. This supports the production of detailed spot maps comprising collections of precise centroid locations vs. frequency and time. Such spot maps have been shown [e.g. in Chen et al., 2015] to delineate complex, fine–scale spatial structure well below the apparent size of individual sources. This capability is new, unique, and scientifically powerful in the context of the science objectives posed above.

Spot maps are frequency– and time–dependent centroid positions valid when the source morphology is dominated by a single, point–like source. This is expected to be the case with solar radio bursts as long as the time–frequency cells are small. Accordingly, both HeRO-S and HeRO-G arrays are designed such that they span comparable physical extents of ∼10 km, corresponding to an accuracy of interferometric phase calibration requirement of 2° and an interferometric signal–to–noise ratio (SNR) of 30. Precise relative calibration benefits from the ability to form closure quantities, requiring a minimum of 3 antennas for phase and 4 for amplitude. The HeRO-S design with 6 antennas provides 10 phase and 9 amplitude closure quantities, and adequate constraints for detecting and modeling simple non-point-like sources in addition to measuring centroid positions. HeRO thereby maintains the required angular precision across the entire 100 kHz to 300 MHz range. To support the scientific goals, HeRO-S and HeRO-G must present a 2D array configuration projected into the solar direction at all times. Furthermore where the structure being observed has an angular extent comparable to or larger than the interferometer fringe spacing, a range of baseline orientations and lengths permits source size to be estimated. HeRO-G stations are designed with true imaging capability, while the 6 HeRO-S spacecraft provide 15 baselines for this purpose.

3 HeRO design

HeRO is a hybrid instrument composed of a ground-based component for frequencies above the ionospheric cut-off (15–300 MHz) and a space-based component covering lower

frequencies not accessible from the ground (100 kHz–20 MHz). Both components operate simultaneously to form a single instrument with frequency coverage from 100 kHz–300 MHz. Both HeRO-S and HeRO-G will make use of the spot mapping technique described in Section 2.2. HeRO could be implemented entirely on a space-based platform, but data storage and clock stability requirements for the higher end of the HeRO frequency band would make the spacecraft unnecessarily complicated and costly. Instead, HeRO-S units are simplified by setting the frequency upper limit at 20 MHz, which maintains overlap with HeRO-G. Position knowledge, sampling rate, and data rate requirements are significantly relaxed at 20 MHz vs. 300 MHz, reducing the cost and complexity of HeRO-S. Both HeRO-S and HeRO-G will record raw voltage data to their respective ring buffers. When an event is identified, either by autonomous triggering (HeRO-G) or by ground–in–the–loop examination of dynamic spectra (HeRO-S), the portion of the buffer containing the event will be frozen and flagged for download or collection. The buffer size on both HeRO segments is sufficiently large for multiple events to be saved while continuing to use the remaining memory in ring buffer mode. HeRO-G events will be used to flag relevant data in the HeRO-S ring buffer and vice versa.

3.1 HeRO-S

HeRO-S(pace) comprises a flock of 6 identical 6U ($30 \times 20 \times 10$ cm^3) CubeSats, each with antenna, receiver, position and timing synchronization, precision clock, and memory management. For interferometry of solar radio bursts, the 6 spacecraft are positioned such that the baselines range from 0.5–10 km, in an optimized 3-D arrangement that is insensitive to slow variations with time. For transient sources like solar radio bursts, traditional aperture synthesis based on evolving baseline projections is not possible, but 'snap–shot' interferometry nevertheless allows precision metrology of centroids for single, compact sources, from which spot maps can be generated as a function of time and frequency.

HeRO-S uses a vector sensor as its antenna. The directivity of the HeRO-S Vector Sensor (VS) (Section 3.3) provides the capability to determine the direction of arrival and the polarization sense of incoming waves, allowing spatial and polarization steering of the antenna beam or nulling of interference sources. This allows HeRO-S to adaptively suppress noise from terrestrial sources by an estimated 30 dB compared to conventional methods, such that solar radio bursts will dominate the result [Knapp et al., 2016a]. Without such nulling capabilities, avoidance of strong terrestrial emissions of both natural and artificial origin would require deployment to a distant location (e.g. Lagrange point or lunar orbit), severely limiting data downlink rates. Positioning HeRO-S above the plasmapause minimizes plasmaspheric masking and distortion over the entire 0.1–20 MHz frequency range while remaining close enough to Earth for efficient high data rate communication.

HeRO-S CubeSats will fly in loose flock in an elliptical, slightly skewed geosynchronous (S-GEO) orbit. The S-GEO orbit provides the benefits of a GEO orbit while never transiting the crowded GEO belt. Requirements for stationkeeping of the spacecraft are not stringent. Knowledge of relative spacecraft position is sufficient to establish array coherence, and can be refined to high accuracy by the interferometry itself. Position knowledge

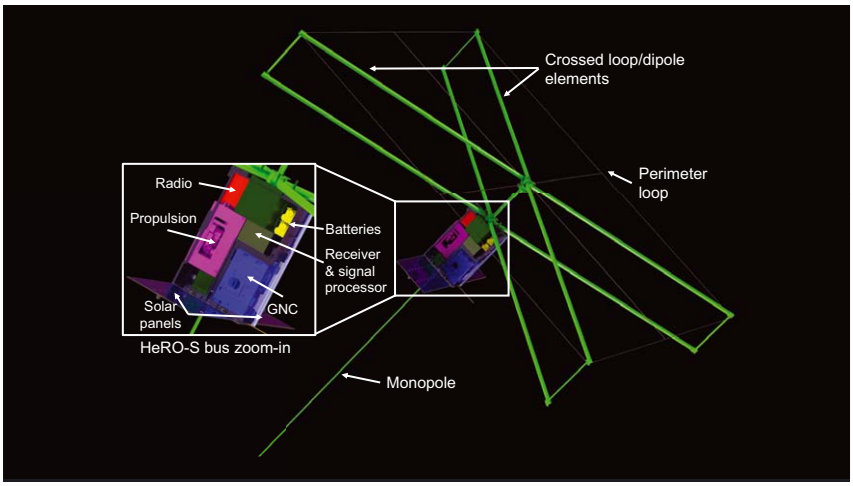

Figure 2: The 6U HeRO-S spacecraft. The vector sensor is composed of two crossed loop/dipole arms, a perimeter loop around the tips of the loop/dipoles, and a monopole. False colors are used to highlight key subsystems. CAD model by M. Silver.

to $1/10$–$1/16$ of a wavelength is generally considered sufficient for interferometric baselines, so HeRO-S's position knowledge requirement is 1–1.5 m at 20 MHz — well within the capability of standard ranging systems. Each spacecraft carries a chip–scale atomic clock for precision timing. Each HeRO-S spacecraft will have a small electric propulsion system for initial orbit adjustment, stationkeeping, reaction wheel desaturation, and disposal at end of life. The stationkeeping requirements for the S-GEO orbit are minimal ($\sim$64 m/s ΔV).

HeRO-S will observe the Sun for 16 hours/day and store raw voltages in a ring buffer which can hold up to 32 hours of data. During the remaining 8 hours, when Earth and the plasmasphere are between the HeRO-S flock and the Sun, HeRO-S will downlink data that has been flagged as containing an event based on ground–in–the–loop examination of summary dynamic spectra from each node. HeRO-S will use a large dedicated X-band ground station to downlink decimated raw data for correlation on the ground rather than cross-correlating in space and downlink the visibilities. Retaining the raw data enables iterative tuning and adjustment of the correlation process for a particular observation, and allows iterative estimation of instrumental calibration parameters. In this respect, the data from both HeRO-S and HeRO-G will allow more processing flexibility than the visibility–only data that is produced by most major observatories.

HeRO-S will be calibrated using a stable NIST–traceable noise diode or comb generator to provide on platform amplitude, frequency, and phase calibration. The calibration signal will be injected into the six antenna inputs [Dicke, 1946; Meloling et al., 2015] to determine channel–to–channel gain and phase differences as well as the absolute gain of the receiver system. The VS antenna element gains as a function of angle are measured by rotation of the spacecraft while observing a known reference such as a ground-based source. Traditional radio interferometry techniques like self–calibration will be used in post–processing on the ground after correlation. To suppress self–electromagnetic interference (EMI), all HeRO subsystems will be selected for low noise and shielded where

necessary. Several spacecraft subsystems, including propulsion and communication, will be turned off during data acquisition. The EMI spectrum will be evaluated throughout development and any affected frequency ranges affected will be constrained where EMI cannot be eliminated entirely.

3.2 HeRO-G

HeRO-G(round) is the ground-based component of HeRO (15–300 MHz). HeRO-G is composed of two geographically separated 'stations', each containing 25 HeRO-G nodes with (U,V) coverage optimized for solar observing (Figure 3, right). Together, the two HeRO-G stations will provide 16+ hours of solar observation per day. The HeRO-G nodes are based on the RAPID (**R**adio **A**rray of **P**ortable **I**nterferometric **D**etectors) node design [Lind et al., 2015]. RAPID is currently under development at MIT Haystack Observatory in collaboration with Cambridge University and NASA JPL. Each RAPID node is physically independent, equipped with a high performance direct digitization receiver, hot–swappable solid state disk (SSD) storage, precision clock, solar and battery power, and optional wireless interconnection.

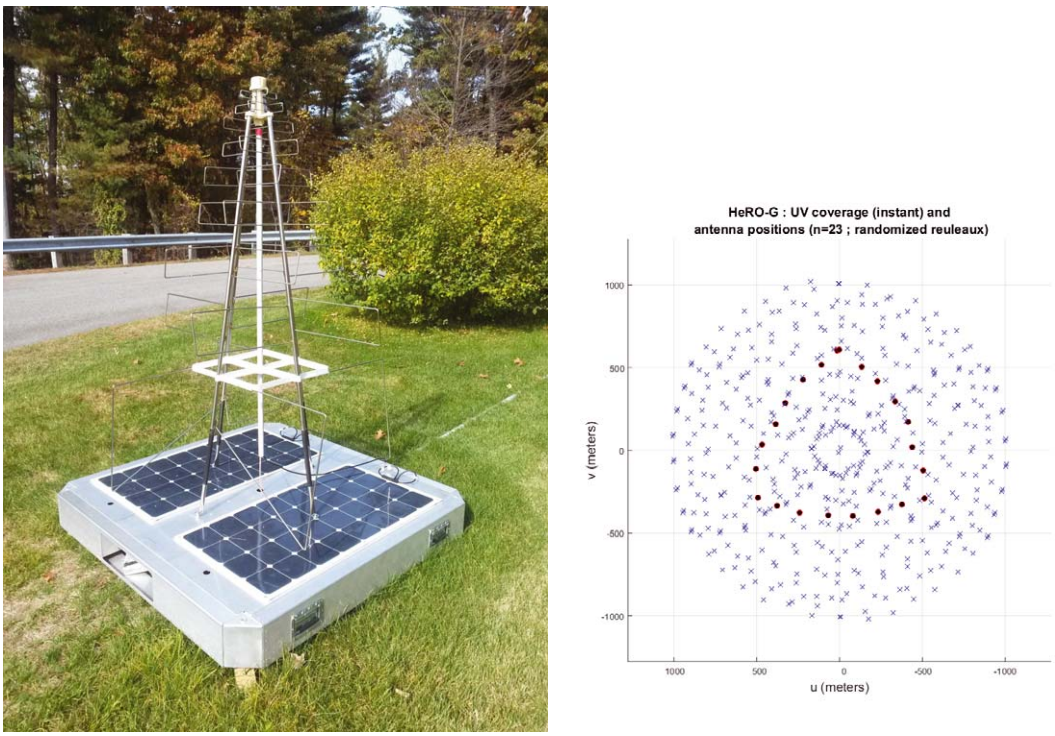

Figure 3: HeRO-G field unit with SKALA antenna (left) and HeRO-G station layout with antenna positions and instantaneous (U,V) coverage (right). There are 25 HeRO-G units per station, arranged in a randomized Reuleaux triangle (red dots) to achieve uniform (U,V) plane filling (blue x). Baseline lengths range from 100 m–10 km.

Each HeRO-G node (Figure 3, left) will use a variant of the SKALA antenna [de Lera Acedo et al., 2015] for 50–300 MHz and a simplified LWA antenna [Ellingson, 2011] for 15–50 MHz. Both antennas will operate simultaneously using a common field unit base.

Raw voltage signals from HeRO-G antennas are captured, filtered, decimated, compressed, and time–tagged before being transferred to the solid state drive (SSD) ring buffer in the HeRO-G base unit.

A subset of HeRO-G nodes will be used as a triggering system that semi–autonomously identifies solar bursts from their compact, transient, and spectrally narrow features and their angular location relative to the solar position. A successful detection causes raw data to be retained locally and a trigger to be sent to the outlying, unconnected nodes via Iridium or other satellite providers. Data are collected manually by swapping the solid state disks and transferring them to a centralized cloud computing facility.

3.3 Vector sensor

A vector sensor is composed of three loops and three dipoles with a common phase center that capture six measurements corresponding to the six components of an electromagnetic wave (3 for E-vector, 3 for B-vector) [Nehorai and Paldi, 1994]. The six elements of the vector sensor allow a complete characterization of incident electromagnetic fields, including full polarization measurement. In the HeRO-S deployable vector sensor, two crossed elements simultaneously provide loop and dipole modes [Robey et al., 2016]. A perimeter loop provides the third loop antenna along with mechanical stability, and a monopole provides the sixth element. The HeRO-S vector sensor, shown in green in Figure 2, is stowed in a 1U volume ($10 \times 10 \times 10$ cm^3) and deployed in orbit. The loop/dipoles are 4 m long, the monopole is 2 m long, the horizontal loop area is 8 m^2 and the two vertical loops are each 1 m^2 [Robey et al., 2016]. Further discussion on vector sensors for astronomical applications can be found in Knapp et al. [2016a], Robey et al. [2016], Knapp et al. [2016b], and Volz et al. [2016].

4 HeRO performance

4.1 Sensitivity

Figure 4 compares HeRO sensitivity with type II and III burst intensities. Even for a single baseline, HeRO-S and HeRO-G have sufficient SNR to detect and characterize nearly all type II and III bursts currently accessible to Wind/WAVES and STEREO over their entire frequency range. More baselines will further improve performance. HeRO's instrumental noise floor is set by the galactic sky noise except at the lowest frequencies. Comparing HeRO's sensitivity or system–equivalent flux density (SEFD, solid black curve in Figure 4) to an average spectrum of a type III burst (dotted red curve) [Saint–Hilaire et al., 2013; Krupar et al., 2014], a signal–to–noise ratio (SNR) of at least 30 is maintained across all frequencies.

Not shown in Figure 4 but of significance is Auroral Kilometric Radiation (AKR), which is due to the electron cyclotron maser instability above Earth's auroral ring. Generally occurring below 500 kHz, AKR is narrowly beamed into frequency–dependent hollow cones aligned with the magnetic field direction in the source region [Mutel et al., 2008;

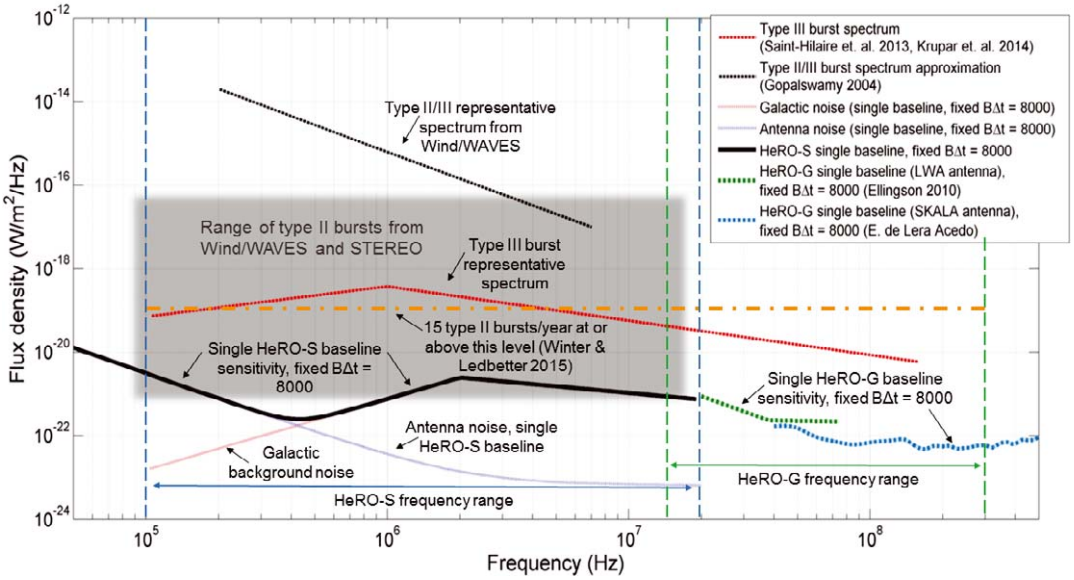

Figure 4: HeRO sensitivity compared with expected solar radio burst flux. A single baseline of HeRO-S or HeRO-G will detect type II and III solar bursts over several decades of intensity and frequency. Shown for comparison are an average type III burst spectrum, scaled to an occurrence rate of 3 bursts per day (red); the range of type II bursts recorded by Wind/WAVES and STEREO over several years (gray box); the intensity of both type II and type II bursts observed by Wind/WAVES (black dashed); HeRO-S SEFD (solid black), the quadrature sum of antenna noise (purple) and galactic background (red) assuming a time–bandwidth product BΔt= 8000; HeRO-G SEFD for LWA antenna (green) and SKALA antenna (cyan). HeRO-G sees substantially less galactic noise than HeRO-S because of the limited field of view.

Menietti et al., 2011], is highly variable, and exhibits modulation with dayside emissions being weaker and less frequent. Time occupancies at the peak frequency of ∼300 kHz are in the 20–40% range [Panchenko et al., 2009]. Fortunately, AKR is strongly beamed away from the equator, is weaker and less frequent during the dayside HeRO-S observations, and is weakest during solar maximum. Any radiation reaching HeRO-S at 6 R_{Earth} will appear compact, on the order of 1°, and can be nulled by the VS.

4.2 Angular resolution

HeRO's astrometric precision is defined in terms of a 'spot', i.e. a datum with position, flux, polarization, time and frequency values at a specific location in this 6D space. Spot position accuracy for a single baseline in one dimension is determined by the fringe spacing

$$\theta = \frac{\lambda}{B} = \frac{103\ arcmin}{\nu_{MHz}},\ B_{max} = 10\ km \tag{1}$$

multiplied by the phase error expressed as a fraction of 2π. This is given by $(2\pi \cdot \mathrm{SNR})^{-1}$, which will vary depending on the radio flux density. For the specified SNR of 30 corre-

sponding to a phase error of 2°, the spot location precision will be

$$\theta = \frac{\lambda}{B \cdot 2\pi SNR} = \frac{0.6\ arcmin}{\nu_{MHz}} \tag{2}$$

This corresponds to 0.03 arcmin at 20 MHz and 6 arcmin at 100 kHz. These accuracies refer to relative measurements between observations nearby in time and frequency, delineating scientifically meaningful structures in the sources. Modeling indicates that 6 CubeSats (15 baselines) meet requirements for all expected sources, while as few as 4 (6 baselines) can locate features with degraded accuracy. HeRO's angular resolution performance is summarized in Figure 5. The angular resolution presented here does not account for source broadening due to scattering; see [Lonsdale et al., 2017].

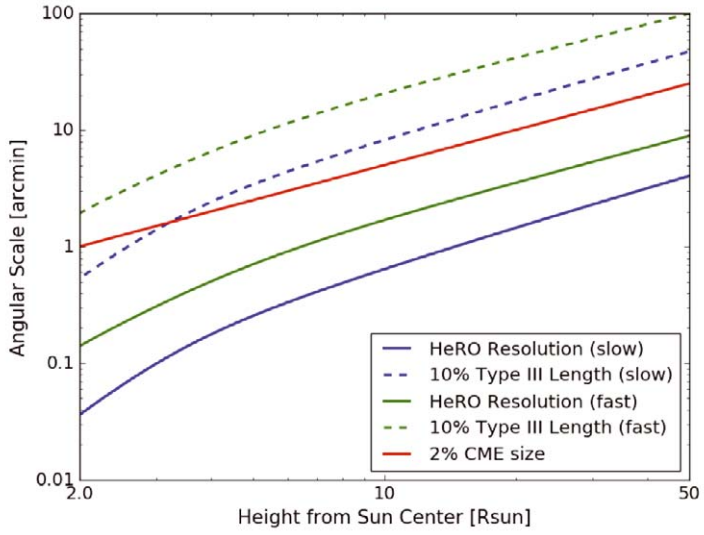

Figure 5: For type II bursts, HeRO-S requires centroid position accuracy <2% of the CME size (red line) [Gopalswamy, 2010]. For type III, HeRO requires 10% of the length of the electron beam based on a burst duration measurement [Alvarez and Haddock, 1973]. Green and blue dashed and solid lines compare modeled accuracy for slow and fast bursts [You et al., 2007].

5 Conclusions

HeRO, alone and in concert with existing and planned in-situ space-based observatories, will significantly enhance understanding of the solar corona, the dynamic interplanetary medium and magnetic field, and particle acceleration processes. In addition to performing groundbreaking heliophysics on its own, HeRO will directly support the in situ measurements of Solar Probe Plus (SPP) and Solar Orbiter (SO) during their cruise phases and close approaches to the Sun.

If HeRO were to launch in early 2022 near the next predicted solar maximum, HeRO is expected to observe 20–40 radio–loud CMEs [Winter and Ledbetter, 2015] and to capture $^2/_3$ of them in its one year life — a sufficient sample to reveal the underlying physics. Type III radio bursts occur much more frequently, providing a sample of many hundreds

to thousands of type III events. HeRO will track type II and III bursts with unprecedented angular and spectral resolution over half of the Earth–Sun distance. Implementation of the HeRO mission would represent a major improvement in angular resolution capability, particularly at low frequencies (HeRO-S). As such, there is strong potential that HeRO will observe previously unknown phenomena in addition to addressing its primary science objectives.

Acknowledgments. The authors thank the extended HeRO team: Ryan Volz, Geoff Crew, Phil Erickson, Alan Fenn, Alex Morris, Mark Silver, Kerry Johnson, Divya Oberoi, Juha Vierinen, Angelos Vourlidas, Stephen White, Kamen Kozarev, Sarah Klein, Sara Seager, Fash Azad, Will Rogers, Tom Brown. We thank the MIT Lincoln Laboratory Advanced Concepts Committee (ACC) for supporting the development of the HF vector sensor for astrophysical applications. The Editors thank Alexander Konovalenko and one anonymous reviewer for their help in evaluating this paper.

References

Alvarez, H., and F. T. Haddock, Decay time of type III solar bursts observed at kilometric wavelengths, *Sol. Phys.*, **30**, 1, 175–182, 1973.

Bastian, T. S, Synchrotron radio emission from a fast halo coronal mass ejection, *Astrophys. J.*, **665**, 1, 805–812, 2007.

Chen, B., T. S. Bastian, C. Shen, D. E. Gary, S. Krucker, and L. Glesener, Particle acceleration by a solar flare termination shock, *Science*, **350**, 6265, 1238–1242, 2015.

Culhane, J. L., D. H. Brooks, L. van Driel–Gesztelyi, P. Démoulin, D. Baker, M. L. DeRosa, C. H. Mandrini, L. Zhao, and T. H. Zurbuchen, Tracking solar active region outflow plasma from its source to the near–Earth environment, *Sol. Phys.*, **289**, 10, 3799–3816, 2014.

de Lera Acedo, E., N. Razavi–Ghods, N. Troop, N. Drought, and A. J. Faulkner, SKALA, a log-periodic array antenna for the SKA–low instrument: Design, simulations, tests and system considerations, *Exp. Astron.*, **39**, 3, 567–594, 2015.

Dicke, R. H., The measurement of thermal radiation at microwave frequencies, *RScI*, **17**, 7, 268–275, 1946.

Domingo, V., B. Fleck, and A. I. Poland, The SOHO Mission: An Overview, in *Solar Phys.*, **162**, 1-2, 1–37, 1995.

Ellingson, S. W., Sensitivity of antenna arrays for long–wavelength radio astronomy, *IEEE Trans. Antennas and Propagation*, **59**, 6, 1855–1863, 2011.

Gary, D. E., and G. J. Hurford, Coronal temperature, density, and magnetic field maps of a solar active region using the Owens Valley Solar Array, *Astrophys. J., Part 1*, **420**, 2, 903–912, 1994.

Gary, D. E., and C. U. Keller, Solar and Space Weather Radiophysics – Current Status and Future Developments, Astrophysics and Space Science Library, **314**, 74, Kluwer Academic Publishers, Dordrecht, The Netherlands, 2004.

Gopalswamy, N., Corona Mass Ejections: A summary of recent results, in *Proc. 20th National Solar Physics Meeting*, Papradno, Slovakia, 108–130, 2010.

Kaiser, M., T. Kucera, J. Davila, O. C. St. Cyr, M. Guhathakurta, and E. Christian, The STEREO mission: An introduction, in *Space Sci. Rev.*, **136**, 1-4, 5–16, 2008.

Knapp, M., F. Robey, R. Volz, F. Lind, A. Fenn, A. Morris, M. Silver, S. Klein, and S. Seager, Vector antenna and maximum likelihood imaging for radio astronomy, in *Proc. IEEE Aerospace Conference*, Vol. 2016–June, 2016a.

Knapp, M., R. Volz, F. D. Lind, F. C. Robey, A. Fenn, K. Johnson, M. Silver, A. Morris, and S. Klein, HF vector sensor for radio astronomy: Ground testing results, in *AIAA SPACE 2016*, American Institute of Aeronautics and Astronautics, Reston, Virginia, USA, 2016b.

Krupar, V., M. Maksimovic, O. Santolik, E. P. Kontar, B. Cecconi, S. Hoang, O. Kruparova, J. Soucek, H. Reid, and A. Zaslavsky, Statistical survey of type III radio bursts at long wavelengths observed by the Solar TErrestrial RElations Observatory (STEREO)/Waves instruments: Radio flux density variations with frequency, *Sol. Phys.*, **289**, 8, 3121–3135, 2014.

Lind, F. D., C. J. Lonsdale, A. J. Faulkner, C. Mattmann, N. Razavi–Ghods, E. de Lera Acedo, P. Alexander, J. Marchese, R. McWhirter, C. Eckert, J. Vierinen, R. Schaefer, W. Rideout, R. Cappallo, V. Pankratius, D. Oberoi, S. Khudikyan, M. Joyce, C. Goodale, M. Boustani, L. Cinquini, R. Verma, and M. Starch, Radio Array of Portable Interferometric Detectors (RAPID): Development of a deployable multiple application radio array, in *2015 ICEAA*, IEEE, 1337–1340, 2015.

Lonsdale, C., L. Benkevitch, I. Cairns, M. Crowley, P. Erickson, M. Knapp, K. Kovarev, F. Lind, P. McCauley, J. Morgan, and D. Oberoi, Solar imaging using low frequency arrays, in *Planetary Radio Emissions VIII*, edited by G. Fischer, G. Mann, M. Panchenko, and P. Zarka, Austrian Academy of Sciences Press, Vienna, 425–434, 2017.

Mann, G., C. Vocks, and F. Breitling, Solar observations with LOFAR, in *Planetary Radio Emissions VII*, edited by H. O. Rucker, W. S. Kurth, P. Louarn, and G. Fischer, Austrian Academy of Sciences Press, Vienna, 507–512, 2011.

Meloling, J., J. W. Rockway, M. P. Daly, A. R. Monges, J. C. Allen, W. R. Nielsen, P. M. McGinnis, R. B. Thompson, and N. A. Mozaffar, An advanced HF direction finding vector–sensing antenna system, SPAWAR System Center Technical Report 2069, 2015.

Menietti, J. D., R. L. Mutel, I. W. Christopher, K. A. Hutchinson, and J. B. Sigwarth, Simultaneous radio and optical observations of auroral structures: Implications for AKR beaming, *J. Geophys. Res.*, **116**, A12219, 2011.

Mutel, R. L., I. W. Christopher, and J. S. Pickett, Cluster multispacecraft determination of AKR angular beaming, *Geophys. Res. Lett.*, **35**, 7, L07104, 2008.

Nehorai, A., and E. Paldi, Vector–sensor array processing for electromagnetic source localization, *IEEE Trans. Signal Processing*, **42**, 2, 376–398, 1994.

Panchenko, M., M. L. Khodachenko, A. G. Kislyakov, H. O. Rucker, J. Hanasz, M. L. Kaiser, S. D. Bale, L. Lamy, B. Cecconi, P. Zarka, and K. Goetz, Daily variations of auroral kilometric radiation observed by STEREO, *Geophys. Res. Lett.*, **36**, 6, L06102, 2009.

Pesnell, W. D., B. J. Thompson, and P. C. Chamberlin, The Solar Dynamics Observatory (SDO), in *Solar Phys.*, **275**, 1-2, 3–15, 2012.

Pohjolainen, S., H. Allawi, and E. Valtonen, Origin of wide-band IP type II bursts, *Astron. Astrophys.*, **558**, id.A7, 19 pp., 2013.

Robey, F., M. Knapp, A. Fenn, M. Silver, K. Johnson, F. Lind, R. Volz, S. Seager, and F. Neylon–Azad, High frequency (HF) radio astronomy from a small satellite, in *Proc. 30th AIAA/USU SmallSat*, 2016.

Saint–Hilaire, P., N. Vilmer, and A. Kerdraon, A decade of solar type III radio bursts observed by the Nançay radioheliograph 1998–2008, *Astrophys. J.*, **762**, 1, id.60, 16 pp., 2013.

Volz, R., M. Knapp, F. Lind, and F. Robey, Covariance estimation in terms of Stokes parameters with application to vector sensor imaging, in *50th Asilomar Conference on Signals, Systems and Computers*, Pacific Grove, CA, USA, 2016.

Winter, L. M., and K. Ledbetter, Type II and type III radio bursts and their correlation with Solar Energetic Proton events, *Astrophys. J.*, **809**, 1, id.105, 19 pp., 2015.

You, X. P., G. B. Hobbs, W. A. Coles, R. N. Manchester, and J. L. Han, An improved solar wind electron density model for pulsar timing, *Astrophys. J.*, **671**, 1, 907–911, 2007.